An Anti-Windup Mechanism for State Constrained Linear Control of Wave Energy Conversion Systems: Design, Synthesis, and Experimental Assessment

An Anti-Windup Mechanism for State Constrained Linear Control of Wave Energy Conversion Systems: Design, Synthesis, and Experimental Assessment

Nicolás Faedo, Fabio Carapellese, Guglielmo Papini, *Graduate Student Member, IEEE*, Edoardo Pasta, *Graduate Student Member, IEEE*, Facundo D. Mosquera, Francesco Ferri, and Ted K. A. Brekken, *Senior Member, IEEE*

***Abstract*—Motivated by the necessity of suitable state constraint mechanisms within linear time-invariant (LTI) energy-maximising control of wave energy converters (WECs), we present, in this article, an anti-windup (AW) scheme for *state* constraint satisfaction, where the associated unconstrained controller is designed via impedance-matching theory for WEC systems. As in the standard (input) AW scenario, the adopted technique provides a mechanism for 'informing' the (unconstrained) controller when constraints are active, so that appropriate modifications to future control actions can be taken accordingly. The overall adopted AW technique is tested experimentally, on a prototype of the Wavestar WEC system, available at Aalborg University (Denmark). We explicitly demonstrate that the proposed AW scheme is able to consistently respect the defined state constraints, having a mild impact on overall energy absorption performance when compared to its unconstrained counterpart.**

***Index Terms*—Wave energy, WEC, anti-windup, impedance-matching, linear control, state constraints.**

I. Introduction

ENERGY-MAXIMISING control design and synthesis for wave energy converters (WECs) can be broadly divided into two main families: optimisation-, and non-optimisation-based techniques [1]. The former family, i.e., optimisation-based strategies, has its foundations in optimal control theory, where typically direct optimal control methods are employed within the WEC research community [2]. These techniques essentially transcribe the associated optimal control problem (OCP) to a corresponding numerically tractable nonlinear program (NP) using diverse approaches, including e.g., model predictive control (MPC) [3], [4], and spectral/pseudospectral methods [5], [6]. A fundamental advantage of optimisation-based techniques is the ability of incorporating technological limitations in terms of state and input constraints, effectively computing optimal policies under constrained conditions. Nonetheless, within this family, regardless of the specific strategy chosen, the resulting NP has to be solved using numerical optimisation routines, often at a large computational expense, potentially compromising real-time implementation.

In contrast, the latter family, i.e., non-optimisation-based controllers, is generally based upon a linear frequency-domain approach to energy-maximisation, leveraging results from so-called *impedance-matching* (maximum power transfer) theory [7], fully avoiding the use of numerical optimisation routines for the computation of the associated control solution. As a matter of fact the adopted control structures, used to realise the associated frequency-domain optimality conditions, commonly stem from linear time-invariant (LTI) system theory, and hence present a notable appeal from an effective practical implementation perspective, being often intuitive in their design and synthesis, with mild computational requirements (see e.g., [8]), being suitable for off-the-shelf hardware implementation.

Though appealing within practical scenarios, in contrast to optimisation-based controllers, which can inherently accommodate state constraints optimally within the computation of the control law, non-optimisation-based controllers share a prevailing Achilles heel: the associated LTI solutions are synthesised in unconstrained conditions. As such, the computed control actions can require physically unfeasible behaviour, very often including excessively large motion. Nonetheless, motivated by the appealing implementation simplicity underlying the family of non-optimisation-based controllers, some solutions have been proposed within the WEC literature to enforce (suboptimally) state constraints. Such proposals are virtually always performed in terms of rudimentary mechanisms, leading to significant performance degradation in terms of energy absorption in practical

Manuscript received 20 April 2023; revised 12 August 2023; accepted 24 September 2023. Date of publication 28 September 2023; date of current version 22 March 2024. This work was supported in part by the European Union's Horizon 020 Research and Innovation Programme through the Marie Sklodowska-Curie under Grant 101024372, in part by framework COST Action 17105 - WECANet, and in part by the Facultad de Ingeniería, Universidad Nacional de La Plata (UNLP), CONICET, and Agencia I+D+i from Argentina. Paper no. TSTE-00418-2023. *(Corresponding author: Nicolás Faedo.)*

Nicolás Faedo, Fabio Carapellese, Guglielmo Papini, and Edoardo Pasta are with the Marine Offshore Renewable Energy Lab, Department of Mechanical and Aerospace Engineering, Politecnico di Torino, 10129 Turin, Italy (e-mail: nicolas.faedo@polito.it; fabio.carapellese@polito.it; guglielmo.papini@polito.it; edoardo.pasta@polito.it).

Facundo D. Mosquera is with the Instituto de Investigaciones en Electrónica, Control y Procesamiento de Senales, Universidad Nacional de La Plata, B1900 La Plata, Argentina (e-mail: facundo.d.mosquera@gmail.com).

Francesco Ferri is with the Department of the Built Environment, Aalborg University, 9220 Aalborg, Denmark (e-mail: ffer@build.aau.dk).

Ted K. A. Brekken is with the Electrical Engineering and Computer Science, Oregon State University, Corvallis, OR 97331 USA (e-mail: brekken@eecs.oregonstate.edu).

Color versions of one or more figures in this article are available at https://doi.org/10.1109/TSTE.2023.3320190.

Digital Object Identifier 10.1109/TSTE.2023.3320190

(constrained) scenarios.[1] Notable examples, sharing this common issue, include e.g., [9], [10]. In particular, [9] re-formulates the control problem into a feedforward reference generation structure, where the provided reference profile is effectively 'saturated' according to the defined limits. [10] utilises a single constant gain to handle state constraints, inherently requiring a) full knowledge of the wave excitation force for tuning, and b) extensive simulation to find a suitable gain value to ensure limit satisfaction.

In the light of the inherent requirement of effective state constraint handling mechanisms for WEC systems, we present, in this article, an anti-windup (AW) scheme for state constraint satisfaction, where the (unconstrained) energy-maximising controller is designed via impedance-matching theory. In essence, AW techniques for this purpose 'transform' the corresponding state constraint set in an equivalent input condition, where relatively standard mechanisms can be considered. This type of structures are known, within the field of control engineering, as *override control* [11], [12], which is essentially akin to AW compensation for the constrained state/output case, rather than constrained inputs. Contemporary approaches for the solution of this problem can be found in e.g., [13], which include rigorous closed-loop stability guarantees, though at the expense of a relatively large set of parameters for effective constraint satisfaction, and an associated iterative procedure for its synthesis. Given that the ultimate objective (and strongest advantage) of non-optimisation-based control for WEC systems, which is the main concern of this article, is that of simplicity of implementation, we propose a state constraint handling procedure based on the strategy in [14] which, as detailed throughout this study, provides a straightforwardly implementable methodology for state constraint satisfaction for a large class of devices. In particular, the contributions of this article are as follows:

- We present an AW setup based on the structure proposed in [14], which can be applied to a general class of non-optimisation-based WEC strategies (see the architectures presented in [7]). The AW scheme incorporates a tailored design for the associated limiting circuit, able to map the defined state constraints into an associated (time-varying) input constraint set.
- Since the effective practical implementation of the proposed AW requires estimation of both the state of the WEC system, and the external uncontrollable input due to the incoming wave field (i.e., the wave excitation force), we incorporate a combined state and input observer based on a Kalman-Bucy filter.
- Finally, the combination of LTI energy-maximising controller, state/input observer, and proposed AW technique, is tested experimentally, using a prototype of the Wavestar WEC system [15], available within the tank-testing facilities of the Ocean and Coastal Engineering Laboratory in Aalborg University, Denmark. Design and synthesis of the constraint handling mechanism is addressed in detail, providing an appraisal of the effect that each main parameter of the strategy has on the overall performance of the controller within experimental implementation. We explicitly demonstrate that the proposed AW scheme is able to consistently respect the defined state constraints, having a mild impact on the overall energy absorption performance when compared to its unconstrained counterpart.

The remainder of this article is organised as follows. Section I-A presents the notation adopted. Section II describes the experimental WEC system considered within this study, while Section III presents the design and synthesis of the (unconstrained) energy-maximising controller via impedance-matching. Section IV describes the proposed AW scheme, including the combined state/input observer considered for effective experimental implementation. Finally, Section V provides an experimental assessment of the overall loop, including extensive performance analysis, while Section VI encompasses the conclusions of this study.

A. Notation

$\mathbb{R}^+$ and $\mathbb{C}^0$ are used to indicate the set of non-negative real numbers, and the set of complex numbers with zero real-part, respectively, while $\mathbb{C}_{<0}$ denotes the set of complex numbers with negative real-part. Given a matrix $A \in \mathbb{C}^{n\times n}$, the notation $\lambda(A) \subset \mathbb{C}$ indicates its set of eigenvalues. The Laplace transform of a function f, provided it exists, is denoted as $F(s)$, $s \in \mathbb{C}$. The Hermitian operator is denoted by $F(\jmath\omega)^\star$, with $\omega \in \mathbb{R}$. The notation $\mathcal{RH}_\infty$ is used for the set of real rational proper and stable functions $G(s)$, $s \in \mathbb{C}$, while $\mathcal{RH}_2$ is considered for the set of strictly proper and stable functions in $\mathbb{C}$. With slight abuse of notation, $\lambda(G(s))$ indicates the set of poles of $G(s)$. The saturation function is defined as $\text{sat}_\Delta(x) = \text{sign}(x)\min(|x|, \Delta)$, $\Delta \in \mathbb{R}^+$, and $x \in \mathbb{R}$. Finally, given a continuous-time signal $g(t)$, its discrete-time zero-order hold equivalent is denoted as $g[k]$, where the sampling time is always clear from the context.

II. Experimental WEC System

The experimental system considered within this study, illustrated in Fig. 1, is a small-scale (1:20) prototype of the Wavestar WEC device [15], tested within the basin facilities available at Aalborg University, Denmark, as part of a larger experimental campaign in WEC modelling and control, executed in September 2022 [16]. The system, which has been previously selected as a benchmark case for WEC control assessment within the first edition of the Wave Energy Control Competition (WEC^{3}OMP) [17], [18], is essentially composed of a floater, connected through an arm to a pivoting point fixed at a reference frame. In the equilibrium position, the arm sits at approximately 30° with respect to the horizontal reference frame. The system is free to move in a single degree-of-freedom, and extracts energy from pitch motion (about the reference point - see Fig. 1) via the corresponding power take-off system (PTO, linear motor/generator) sitting on the upper structural joint of the device arm. Though we avoid a full description of each of

[1]The reader is referred to [8] for a detailed discussion on constraint handling capabilities within the state-of-the-art of LTI WEC controllers.

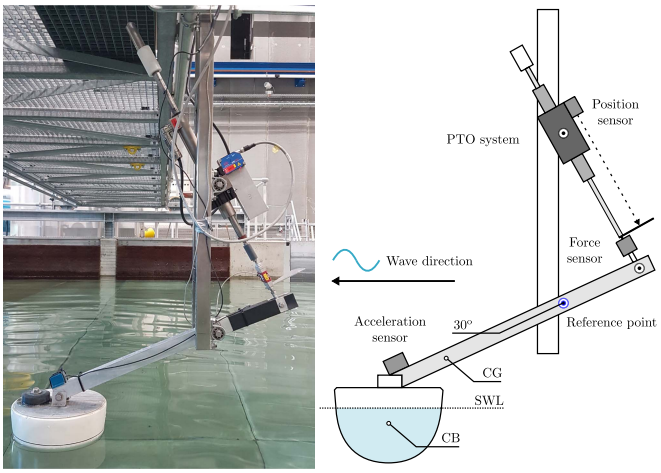

Fig. 1. Experimental prototype of the Wavestar system (left) and corresponding schematic (right). SWL, CG and CB stand for still water level, center of gravity, and center of buoyancy, respectively.

the WEC components for economy of space, we refer the reader to [17] for further detail.

The wave tank facilities, considered within this experimental campaign, are those available at the Ocean and Coastal Engineering Laboratory at Aalborg University, Denmark. In particular, the available facilities comprise a basin of 19.3 [m] $\times$ 14.6 [m] $\times$ 1.5 [m] (length $\times$ width $\times$ depth), with an active testing area of 13 [m] $\times$ 8 [m] (length $\times$ width). The wave tank is equipped with a state-of-the-art long-stroke segmented wavemaker system with active absorption, composed of 30 individually controlled wave paddles, capable of producing a large variety of sea state conditions with high accuracy. Within this study, the water depth within the tank has been fixed to 0.9 [m], while the wavemaker is set to generate long-crested waves, i.e., parallel with respect to (w.r.t.) the y-axis, and with a direction of 0° on the x-axis.

A measure of pitch motion about the reference point is available via a combination of a dedicated laser position sensor (located at the PTO axis), and a dual-axis accelerometer, sitting on top of the floater (see Fig. 1). Data acquisition and control are implemented with a target Speedgoat real-time hardware using a UDP protocol, connected to a host PC running Matlab Simulink via a local Ethernet network. Acquisition is consistently performed at a sampling rate of 200 [Hz], for all the acquired variables, within the totality of the experimental campaign.

III. Energy-Maximising Control Design

Throughout this study, and adopting the very same arguments posed within the WEC^{3}OMP [17], we assume that the prototype WEC system, described in Section II, can be modelled in terms of a representative linear operator $G(s) = C(s\mathbb{I}_n - A)^{-1}B \in \mathcal{RH}_2$, defined in terms of a minimal state-space realisation as

$$G(s) \equiv \begin{cases} \dot{x}(t) = Ax(t) + B(d_\theta(t) + u_\theta(t)), \\ y_\theta(t) = Cx(t), \end{cases} \tag{1}$$

with $(A, B, C^{\mathsf{T}}) \in \mathbb{R}^{n\times n} \times \mathbb{R}^n \times \mathbb{R}^n$, and where $G(s)$ is of relative degree 1. Note that, equivalently, (1) characterises the input-output (I/O) relation

$$Y_\theta(s) = G(s)\left(D_\theta(s) + U_\theta(s)\right), \tag{2}$$

where y_θ is the device (pitch) velocity about the reference point (see Fig. 1), d_θ is the (uncontrollable) wave excitation torque due to the action of the wave field on the floater wetted surface, and u_θ is the control torque, supplied via the corresponding PTO system.

Remark 1: We note that, due to the physics associated with the WEC process, the map G in (2) is also minimum-phase. Furthermore, the transfer function $G(s)$ is positive real, and hence the associated system (1) is passive (see [7], [19]).

Following the requirement of energy-maximisation in WEC systems, the PTO control force u_θ in (2) is to be designed such that the following map (control objective),

$$u_\theta = \arg\max_{u_\theta} -\int_{-\infty}^{+\infty} u_\theta\, y_\theta \,\mathrm{d}t, \tag{3}$$

is maximised, i.e., such that maximum mechanical energy absorption from the wave field is effectively achieved by the corresponding controller. Adopting a frequency-domain approach, the optimal control solution u_θ for (3) can be derived via the so-called impedance-matching principle [7] (also known as maximum power transfer theorem), where the WEC system is essentially described in terms of an *impedance*, analogously to standard circuit theory. Briefly summarising, let $I(\jmath\omega)$ be the *impedance* of the prototype WEC system, defined, in the frequency domain, as[2]

$$I(\jmath\omega) = \frac{1}{G(\jmath\omega)}. \tag{4}$$

With the definition in (4), the (frequency-domain) optimal control solution (*load*), can be simply written in terms of the complex conjugate of I, as

$$U_\theta(\jmath\omega) = -I(\jmath\omega)^\star Y_\theta(\jmath\omega), \tag{5}$$

which is, in essence, an output feedback structure.

Remark 2: Though one can be tempted to use the analytic continuation of $I^\star$ to $\mathbb{C}$, in order to implement the control structure in (5), the resulting transfer function is inherently *non-causal*, due to the nature of the analytic continuation of the Hermitian operator (see the arguments posed in e.g., [19]).

Remark 2 refers to a well-known issue in the design and synthesis of wave energy control systems. One can, although, approximate condition (5) by employing tailored causal and stable control structures, i.e., implementable. In particular, within this study, we consider a first-order biproper controller $K(s) \in \mathcal{RH}_\infty$, defined as

$$K(s) = \frac{\alpha_1\, s}{s + \alpha_2}, \tag{6}$$

where the set of parameters $\mathscr{A} = \{\alpha_1, \alpha_2\}$ are uniquely computed as the solution of the interpolation equation

$$K(\jmath\omega_{\mathcal{I}}) = I(\jmath\omega_{\mathcal{I}})^\star, \tag{7}$$

[2]Note that, due to the dynamical properties of the WEC system described within this section, $G(\jmath\omega)^{-1}$ is well-defined for any $\omega \in \mathbb{R}/0$.

with $\omega_{\mathcal{I}} \in \mathbb{R}^+$ a suitably selected interpolation frequency.

Remark 3: Typically, within the vast majority of impedance-matching-based control for WECs, proportional-integral (PI) structures are considered to achieve (7) (see e.g., [20]), often simply motivated by their use in more to achieve more 'standard' control objectives (i.e., regulation). Nonetheless, the design of K in terms of a PI structure via the interpolation condition (7) does not guarantee, in general, closed-loop stability. Furthermore, negative values for the integral term are often required to achieve (7) (known in the WEC community as a 'negative stiffness' term), leading to non-minimum-phase behaviour. In contrast, (6) provides, for the device under study, a stable and minimum-phase structure achieving (7) (see also Remark 5). This, together with the passivity property associated with the WEC system (1) (see Remark 1), guarantees closed-loop stability in nominal (unconstrained) conditions.

Remark 4: The control structure in (6) interpolates the optimal load in (5) for a single frequency point $\omega_{\mathcal{I}}$, which needs to be selected according to the nature of the wave field. Common choices for $\omega_{\mathcal{I}}$ include the frequencies associated with peak and energetic wave periods.

Remark 5: For the case of the prototype WEC system considered, the set $\mathscr{A} \subset \mathbb{R}^+$ (see also Section V), and hence (6) is both stable and minimum-phase.

IV. State-Constraint Handling

Within this section, we introduce the adopted AW scheme for state constraint satisfaction, tailored for the WEC prototype presented in Section II, and the control structure defined in Section III. Throughout this section, we consider the discrete-time equivalents $\{G_{\mathrm{d}}(q), K_{\mathrm{d}}(q)\}$ (with q the forward-shift operator) corresponding with the transfer functions $G(s)$ and $K(s)$ in equations (2) and (6), respectively, computed via a standard zero-order hold procedure with a sufficiently small sampling time $T_{\mathrm{s}} \in \mathbb{R}^+$. Furthermore, we write G_{d} in terms of a state-space realisation

$$G_{\mathrm{d}}(q) \equiv \begin{cases} x[k+1] = A_{\mathrm{d}}x[k] + B_{\mathrm{d}}\left(d_\theta[k] + u_\theta[k]\right), \\ y_\theta[k] = C_{\mathrm{d}}x[k], \end{cases} \tag{8}$$

where the triple of matrices $(A_{\mathrm{d}}, B_{\mathrm{d}}, C_{\mathrm{d}})$ can be computed directly from (1). We further assume that (8) is subject to a set of state constraints defined in terms of the velocity y_θ, i.e.,

$$y_\theta[k] = C_{\mathrm{d}}x[k] \in \mathbb{Y} \triangleq [-\Delta, \Delta], \tag{9}$$

with $\Delta \in \mathbb{R}^+$, $\forall k \in \mathbb{N}$. We note that, within this article, we assume that sufficient PTO force is effectively available to constraint the state behaviour of the system according to (9), i.e., that the constrained problem is effectively feasible. We refer the reader to [21] for further detail on feasibility for generic WEC systems.

Remark 6: Constraints in angular velocity are chosen as a representative case for the experimental assessment proposed within this study, due to the intrisic connection between y_θ and optimal mechanical energy absorption (see equation (3)). Nonetheless, we note that this is done without loss of generality, and any other constraint of the form $\{x \in \mathbb{R}^n | \, Cx \in \mathscr{C}\}$ can be considered within the presented procedure.

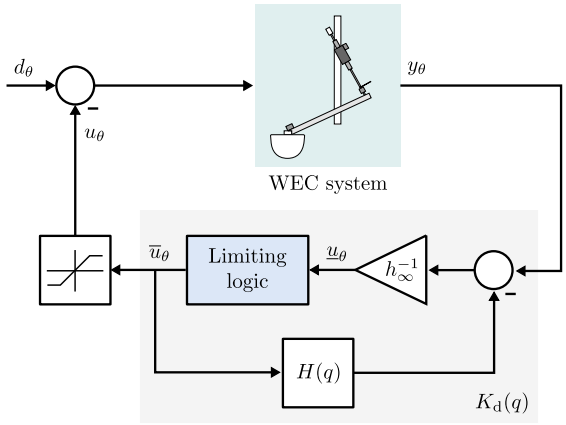

Fig. 2. General AW scheme for input constraints, as considered in [14].

Fig. 2 illustrates a general scheme for AW in the (standard) case of input constraints (see e.g., [22]). In particular, following an analogous procedure to that in [14], and given that the controller K_{d} is biproper, stable, and minimum-phase (see Remark 5), we can decompose its transfer function as

$$K_{\mathrm{d}}(q)^{-1} = h_\infty + H(q), \tag{10}$$

where h_∞ is the high frequency gain of $K_{\mathrm{d}}(q)^{-1}$, and $H(q)$ is both stable and strictly proper.

Remark 7: By replacing the limiting logic block in Fig. 2 by a unitary function, it is straightforward to see that the closed-loop response of the AW block is, effectively, $K_{\mathrm{d}}(q)$.

Focusing on the development of an AW scheme for the WEC state constraint case, we note that the set $\mathbb{Y}$ can be defined in terms of a corresponding input constraint set $\mathbb{U}$, i.e., we write the state limitation (9) for y_θ in terms of an equivalent restriction in u_θ. The latter set, i.e., $\mathbb{U}$, although, is inherently time-varying, as discussed in the following. Consider system (8) subject to the state constraint in (9). Since G_{d} is strictly proper with relative degree 1, a one-step ahead prediction of y_θ can be computed as

$$y_\theta[k+1] = C_{\mathrm{d}}A_{\mathrm{d}}x[k] + C_{\mathrm{d}}B_{\mathrm{d}}\left(d_\theta[k] + u_\theta[k]\right), \tag{11}$$

where $\mathbb{R} \ni C_{\mathrm{d}}B_{\mathrm{d}} \neq 0$. Solving for u_θ in (11), we can define the following transition map $\Gamma : \mathbb{R} \times \mathbb{R}^n \times \mathbb{R} \to \mathbb{R}, (y_\theta, x, d_\theta) \mapsto \Gamma(y_\theta, x, d_\theta)$,

$$\Gamma(y_\theta, x, d_\theta) = \left(C_{\mathrm{d}}B_{\mathrm{d}}\right)^{-1}\left(y_\theta - C_{\mathrm{d}}A_{\mathrm{d}}x\right) - d_\theta. \tag{12}$$

Note that the function Γ, as defined in (12), can be effectively used to map the state constraint set $\mathbb{Y}$ to an equivalent time-varying input constraint set $\mathbb{U}(x, d_\theta) = \Gamma(\mathbb{Y}, x, d_\theta)$. In particular, for a given value of y_θ, the induced input constraint set can be explicitly written as

$$\mathbb{U} \triangleq \left[\Delta^{\mathrm{l}}(x, d_\theta), \Delta^{\mathrm{u}}(x, d_\theta)\right] \subset \mathbb{R}, \tag{13}$$

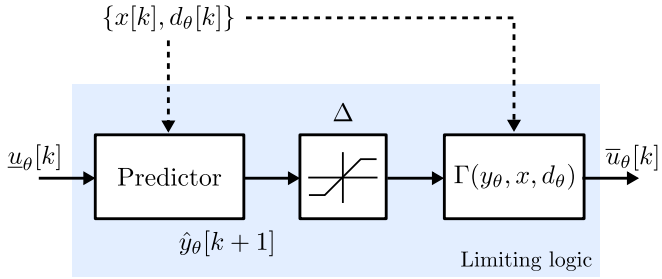

Fig. 3. Adopted AW limiting logic.

with

$$\Delta^{\mathrm{l}}(x, d_\theta) = (C_{\mathrm{d}} B_{\mathrm{d}})^{-1} (-\Delta - C_{\mathrm{d}} A_{\mathrm{d}} x) - d_\theta,$$
$$\Delta^{\mathrm{u}}(x, d_\theta) = (C_{\mathrm{d}} B_{\mathrm{d}})^{-1} (\ \Delta - C_{\mathrm{d}} A_{\mathrm{d}} x) - d_\theta, \qquad (14)$$

where, clearly, it follows that $y_\theta \in \mathbb{Y} \Leftrightarrow u_\theta \in \mathbb{U}, \forall k \in \mathbb{N}$.

With the time-varying set derived in (14), an AW scheme, effectively able to handle the state constraint $\mathbb{Y}$ in (9), can be defined in terms of the limiting logic presented in Fig. 3. In particular, the adopted AW is, in essence, a two-step procedure, which can be summarised as follows:

- Let $x[k]$ and $d_\theta[k]$ be the current state of system (8) and wave excitation input, respectively, and $\underline{u}_\theta[k]$ the control law required by the controller K_{d}. A one-step prediction $\hat{y}_\theta[k+1]$ can be computed via (11).
- Constraint violations in accordance with the set $\mathbb{Y}$ are subsequently detected in the prediction $\hat{y}$ by applying the saturation map $\mathrm{sat}_\Delta(\cdot)$. Based on the saturated value of $\hat{y}[k+1]$, an allowed control action $\overline{u}_\theta[k]$ can be back-calculated using the map $\Gamma(\cdot, x, d_\theta)$ in (12).

Remark 8: Clearly, if no constraint violation is detected, $\underline{u}_\theta = \overline{u}_\theta$, i.e., the unconstrained control solution, associated with the energy-maximising controller K_d, is directly applied to the WEC. If, on the contrary, the constraint on y_θ is active, $\overline{u}_\theta$ takes y_θ to the limit of the set $\mathbb{Y}$.

A. Combined State and Unknown-Input Estimation

Effective implementation of the AW structure, detailed within Section IV, requires instantaneous knowledge of the state-vector x and the wave excitation torque d_θ, in order to effectively back-calculate admissible control actions via (12). Since both quantities are virtually always unmeasurable (see the arguments in e.g., [23]), we leverage results from unknown-input estimation to provide suitable estimates of both x and d_θ, denoted as $\widetilde{x}$ and $\widetilde{d}_\theta$, respectively. In particular, guided by the performance results for wave excitation observers presented in [23], we consider a (steady-state) Kalman-Bucy filter [24] in combination with an internal (approximate) model of d_θ.

Remark 9: A continuous-time formulation of the unknown-input observer is considered herein, due to its use within the literature of wave energy estimation and control [23]. Nonetheless, we note that a discrete formulation can be effectively considered accordingly, leveraging the discrete-time equivalent presented in (8).

To be precise, we describe the wave excitation force in terms of the following exogenous dynamical system[3]

$$\begin{cases} \dot{\xi}_\theta(t) = S_\theta \xi_\theta(t) \\ d_\theta(t) = L_\theta \xi_\theta(t), \end{cases} \text{ with } S_\theta = \bigoplus_{i=1}^{p} \begin{bmatrix} 0 & \omega_i \\ -\omega_i & 0 \end{bmatrix} \in \mathbb{R}^{\kappa \times \kappa}, \qquad (15)$$

$\kappa = 2p$, $\mathscr{F} = \{\omega_i\}_{i=1}^{p} \subset \mathbb{R}^+$ a set of descriptor frequencies, chosen according to the input wave spectrum, and where $L_\theta^{\mathsf{T}} \in \mathbb{R}^\kappa$ is such that the pair (S_θ, L_θ) is observable. Based on (15), we define the 'extended' dynamical system

$$\begin{cases} \dot{x}_f(t) = A_f x_f(t) + B_f u_\theta(t) + \varepsilon_{x_f}(t), \\ y_\theta(t) = C_f x_f(t) + \varepsilon_{y_\theta}(t), \end{cases} \qquad (16)$$

where $x_f(t) = [x(t)^{\mathsf{T}} \ \xi_\theta(t)^{\mathsf{T}}]^{\mathsf{T}} \in \mathbb{R}^{\tilde{n}}$, with $\tilde{n} = n + \kappa$, and $\varepsilon_{x_f}(t) \in \mathbb{R}^{\tilde{n}}$ and $\varepsilon_{y_\theta}(t) \in \mathbb{R}$ represent (white, zero-mean, mutually uncorrelated) process and measurement noise, respectively, with associated covariance matrices $Q_f \in \mathbb{R}^{\tilde{n} \times \tilde{n}}$ and $R_f \in \mathbb{R}$. The triple $(A_f, B_f, C_f^{\mathsf{T}}) \in \mathbb{R}^{\tilde{n} \times \tilde{n}} \times \mathbb{R}^{\tilde{n}} \times \mathbb{R}^{\tilde{n}}$ in (16) is given by

$$A_f = \begin{bmatrix} A & BL_\theta \\ 0 & S_\theta \end{bmatrix}, \quad B_f = \begin{bmatrix} B \\ 0 \end{bmatrix}, \quad C_f = \begin{bmatrix} C & 0 \end{bmatrix}. \qquad (17)$$

The observer is hence given in terms of the following classical Luenberger structure

$$\begin{cases} \dot{\widetilde{x}_f}(t) = (A_f - L_f C_f) \widetilde{x_f}(t) + L_f y_\theta(t) + B_f u_\theta(t), \\ \widetilde{x}(t) = \begin{bmatrix} \mathbb{I}_n 0 \ \end{bmatrix} \widetilde{x_f}(t), \\ \widetilde{d_\theta}(t) = \begin{bmatrix} 0 L_\theta \ \end{bmatrix} \widetilde{x_f}(t), \end{cases} \qquad (18)$$

where the observer gain in (18) can be computed as $L_f = P_f C_f^{\mathsf{T}} R_f^{-1}$, with $P_f = P_f^{\mathsf{T}} \in \mathbb{R}^{\tilde{n} \times \tilde{n}}$ the unique solution of the continuous-time algebraic Riccati equation

$$A_f P_f + P_f A_f^{\mathsf{T}} - P_f C_f^{\mathsf{T}} R_f^{-1} C_f P_f + Q_f = 0. \qquad (19)$$

B. Smooth Approximation of the Saturation Map

To avoid any abrupt requirements in terms of PTO (actuator) action, and hence ease the practical experimental implementation of the AW scheme proposed, we consider a smooth approximation of the saturation map $\mathrm{sat}_\Delta(\cdot)$. In particular, given $z \in \mathbb{R}$, we first note that a smooth approximation of the absolute value function in terms of a single parameter $\epsilon \in \mathbb{R}^+$ can be obtained as

$$|z| \approx |z|_\epsilon = \sqrt{z^2 + \epsilon^2}, \qquad (20)$$

where, clearly, $\lim_{\epsilon \to 0} |z|_\epsilon = |z|$. With the expression in (20), an approximation of the saturation function can be readily computed as

$$\mathrm{sat}_\Delta(z) \approx \frac{1}{2} \Big(|z + \Delta|_\epsilon - |z - \Delta|_\epsilon \Big), \qquad (21)$$

with ϵ sufficiently small. Fig. 4 illustrates the approximation provided by (21), for a value $\Delta = 0.4$ (which is effectively

[3]The harmonic-based description of ocean waves is well-established within the WEC control/estimation literature, and has been exploited in numerous studies (see e.g., [25]).

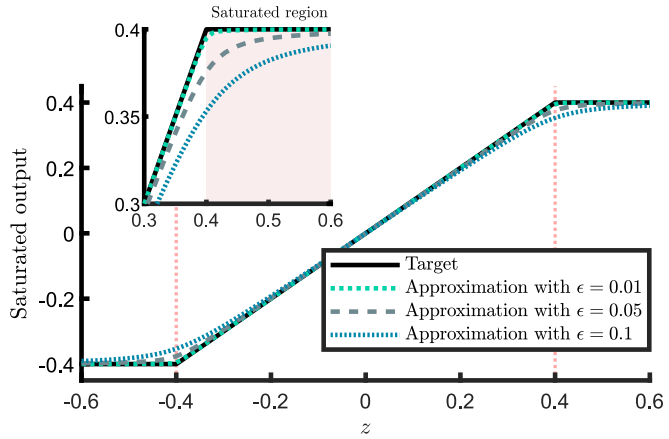

Fig. 4. Smooth approximation of $\text{sat}_{\Delta}(\cdot)$.

consistent with the saturation value adopted in the experimental assessment of Section V), and three different values of $\epsilon \in \{0.01, 0.05, 0.1\}$.

As it can be appreciated, a larger value of ϵ generates a 'smoother' transition between a non-saturated and saturated state. This inherently implies, although, that the corrective AW action is effectively applied for smaller values than those characterising the actual hard constraint Δ, i.e., the AW loop is more conservative for higher values of ϵ, which can have an impact on the energy-maximising capabilities of the overall loop, as explicitly demonstrated within the experimental evaluation of the technique presented in Section V.

V. Experimental Results

We present, in this section, an experimental assessment of the AW scheme detailed in Section IV, comprising the energy-maximising control design as in Section III, and applied to the prototype described in Section II. For performance assessment, we consider an irregular sea-state characterised in terms of a JONSWAP spectrum, with a significant wave height $H_{\text{s}} = 0.063$ [m], typical peak period $T_{\text{p}} = 1.412$ [s], and peak enhancement factor $\gamma = 3.3$. We note that this sea-state corresponds with sea-state N °5 of the WEC^3 OMP (see [17], [18]). The wave (i.e., experiment) duration is set to 300 [s], which corresponds with more than 150 typical peak periods, hence guaranteeing statistically consistent results for the performance assessment in terms of energy absorption. The sampling time, considered both for data-acquisition, and corresponding discretisation of system/controller, is set to $T_{\text{s}} = 0.005$ [s] (rate of 200 [Hz]), as per the discussion provided in Section II.

Within this study, the WEC model (1), characterising the behaviour of the experimental prototype, is obtained using black-box system identification procedures. To summarise, analogously to the experimental study presented in [26], a set of down-chirp signals with different amplitudes (in the interval [1,4] [Nm]) is injected into the PTO system as input (torque) signals (in calm waters, i.e., in absence of waves within the basin), generating a corresponding set of output (velocity) responses. Each I/O pair is used to compute a frequency-domain empirical

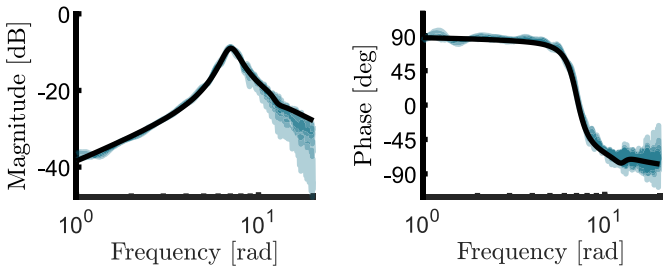

Fig. 5. Frequency-domain identification results. The solid line illustrates the computed model, while each transparent line corresponds to a single I/O experiment.

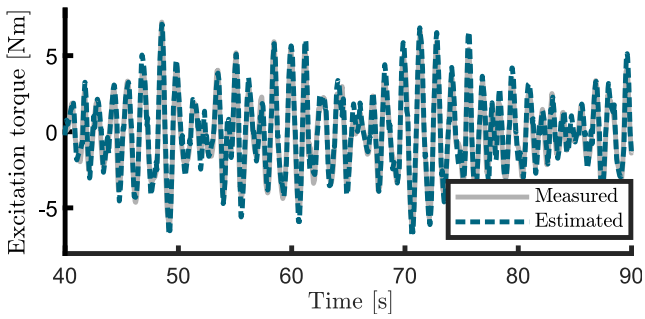

Fig. 6. Appraisal of the wave excitation torque estimation.

transfer function estimate [27], and their corresponding average is used as target data-set for subspace-based identification [28], [29]. The result of the described system identification procedure can be appreciated in the Bode plot presented in Fig. 5. The obtained state-space model is of order (dimension) $n = 8$, and is effectively compliant with all the main physical properties relative to the WEC process (internal stability, relative degree, and minimum-phase).

With respect to the energy-maximising controller $K(s)$, as defined in equation (6), the interpolation frequency $\omega_{\mathcal{I}}$ is chosen in terms of the energetic period associated with the sea-state considered, i.e., $\omega_{\mathcal{I}} = 2\pi/(0.9T_{\text{p}})$ producing a corresponding set of parameters $\alpha_1 = 14.41$ and $\alpha_2 = 5.11$.

Regarding the estimation of both state and wave excitation input (as proposed within Section IV-A), required for the implementation of the proposed AW technique, the matrix S_θ in (15), describing the internal model of d_θ, is such that $\mathscr{F} = \{2\pi/1.412, 2\pi/1.836, 2\pi/0.988\}$. Note that the first value within the set $\mathscr{F}$ corresponds to the frequency associated with the typical peak period of the sea-state considered within this study, while the other two values have been chosen via extensive simulation. The matrices characterising the design and tuning of the adopted Kalman-Bucy observer are chosen as $Q_f = 20\mathbb{I}_{\tilde{n}}$ and $R_f = 0.1$. To illustrate the performance of the estimator, Fig. 6 shows a snippet of the target wave excitation force d_θ (measured in a separate experiment by externally locking the device and measuring the force exerted by the incoming wave - see e.g., [26]), and estimated signal $\widetilde{d_\theta}$. It can be appreciated that the estimation provided by the observer

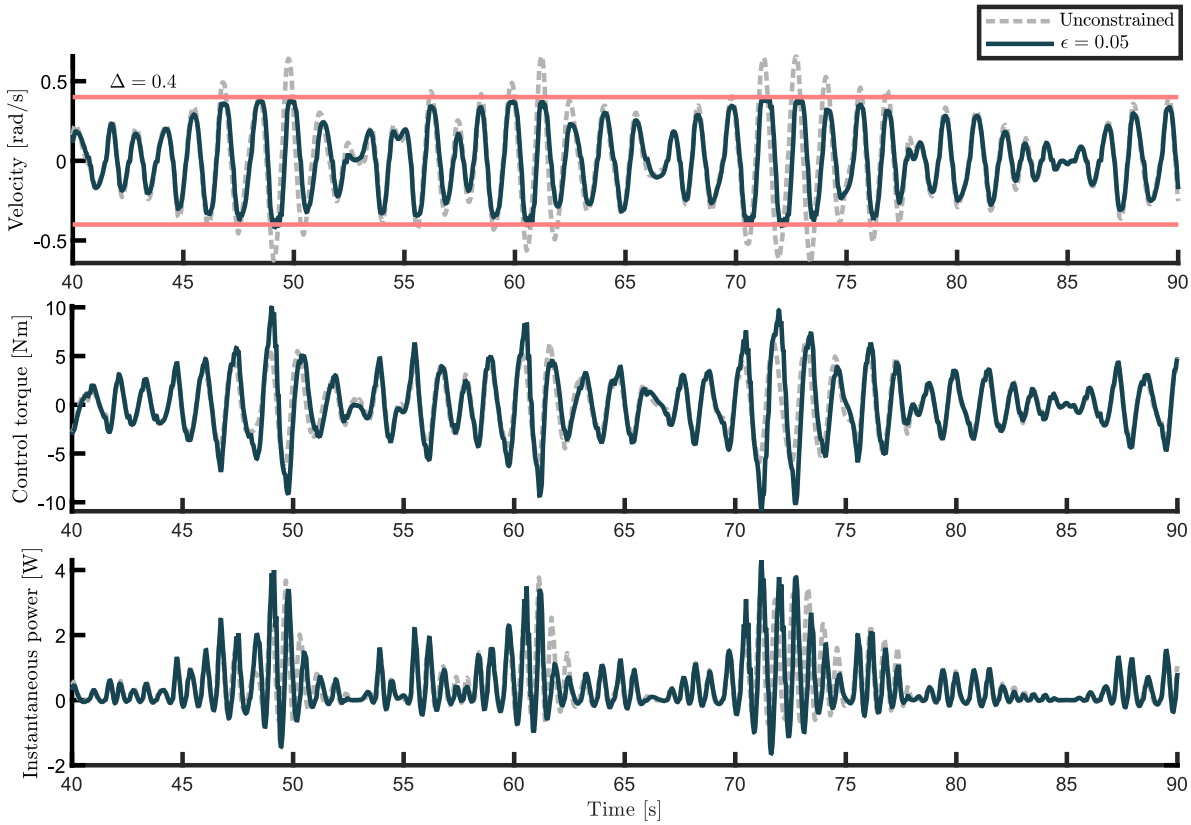

Fig. 7. Experimental WEC motion and associated control input for both unconstrained, and state-constrained AW case.

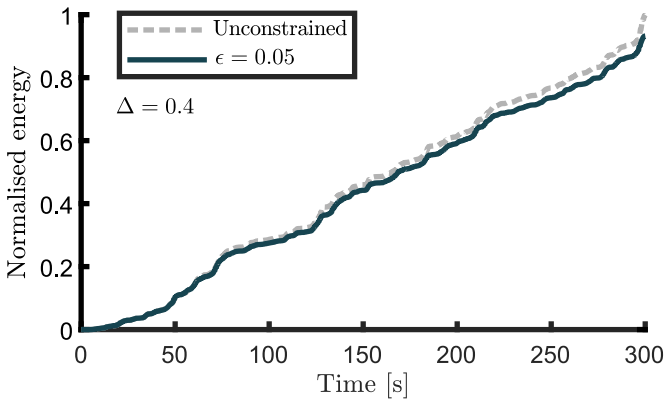

Fig. 8. Absorbed mechanical energy.

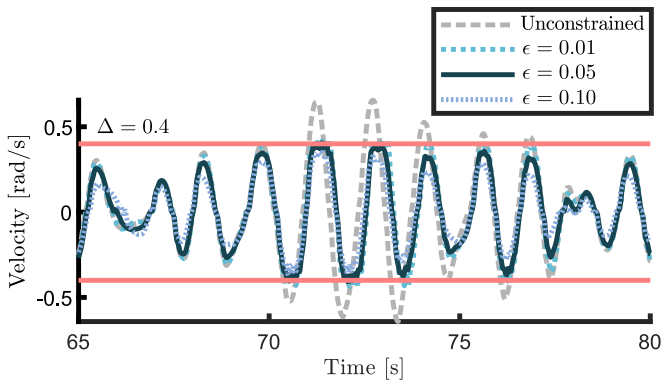

Fig. 9. Comparison in terms of output velocity for different values of ϵ.

is effectively highly accurate, having a mean normalised error of ≈ 0.10.

Concerning the specifics associated with the state AW scheme itself, the constraint set $\mathbb{Y}$, characterising the state limitation in (9), is set to $\Delta = 0.4$ [rad/s]. Note that this value is effectively conservative for this device (and sea-state), and has been chosen to clearly illustrate the capabilities of the proposed state AW in experimental scenarios, under potentially severe constraint limits. The saturation block, used within the limiting logic in Fig. 3, is approximated as in Section IV-B, with a nominal value of $\epsilon = 0.05$ (see Fig. 4).

The results of applying the proposed AW scheme can be appreciated in Fig. 7, where both the unconstrained (dashed), and constrained (solid), output response of the WEC are illustrated (top), together with each associated control input (middle), and instantaneous mechanical power (bottom). Note that both responses are obtained in separate experiments using the same wave realisation, being the former only driven by the unconstrained controller $K(s)$, while the latter effectively incorporates the proposed AW, with all its components (i.e., energy-maximising controller, state/input observer, and associated constraint satisfaction logic). It can be straightforwardly

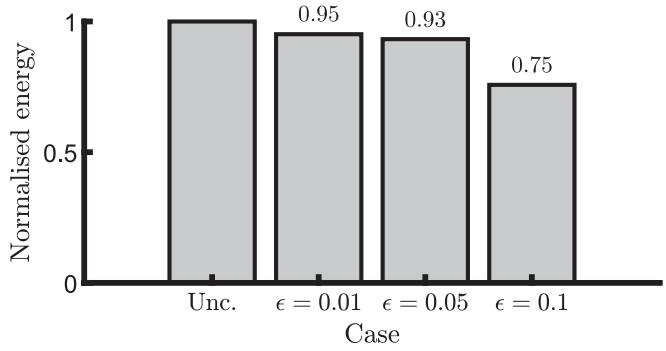

Fig. 10. Mechanical energy absorption for different values of ϵ.

seen that the AW technique is effectively able to enforce the imposed state constraint, being always within the specified limit, while the unconstrained controller consistently violates the maximum velocity value. Furthermore, as expected from the arguments posed in Remark 8, the AW strategy provides an input correction *only* when the system is close to attaining the constraint limit, by requiring an 'extra' torque to assist constraint satisfaction, yet being virtually the same as the unconstrained energy-maximising solution when the state constraint is not active. This 'extra' component generates an associated instantaneous power flow, which can be seen to be slightly more reactive at the time instants in which the AW logic is effectively active (i.e., device moving with a velocity inside the saturation region).

Remark 10: Though small differences can be noted between unconstrained and constrained control solutions when the state constraint is inactive, these can be explained by the fact that both controllers are tested in separate experiments, where the same wave has to be realised by the associated wavemaker, which, although highly repetitive, presents slight differences in terms of effective wave generation.

Fig. 8 presents an appraisal in terms of energy absorption, showing that the AW, as tuned and designed within this section, has a minimum influence on the overall loop performance, by virtue of the specific limitation logic, which modifies the unconstrained optimal solution only when strictly necessary.

Finally, and to provide an appraisal of the effect of ϵ in the overall behaviour of the proposed AW solution and associated energy absorption performance, Fig. 9 presents motion (angular velocity) of the device for $\epsilon = \{0.01, 0.05, 0.1\}$, which produces the set of saturation approximation functions in Fig. 4. As can be appreciated from this figure, consistently with the discussion provided in Section IV-B, a higher value of ϵ results in a smoother device response, though with an overall more conservative constraint handling mechanism, potentially interfering with the energy-maximising control objective of the unconstrained controller $K(s)$. This last statement is clear in Fig. 10, where the energy absorption is effectively reduced significantly when epsilon is 0.1 (i.e., the largest value within the set), being $\approx 75\%$ of the energy obtained in the unconstrained scenario. On the other end, a small value of ϵ can require an abrupt control action from the PTO system, exerting a potentially demanding fatigue on the corresponding actuator, though with a consequent increase in energy absorption capabilities (see Fig. 9).

VI. Conclusion

We present, in this article, an AW scheme for state constraint handling in LTI energy-maximising control of WEC systems. The technique, which can be applied to a general class of non-optimisation-based WEC control strategies, provides a mechanism for 'informing' the (unconstrained) controller when state constraints are active, so that appropriate modifications to future control actions can be taken accordingly. Furthermore, since effective practical implementation of the proposed AW requires estimation of both the state of the WEC system, and the external uncontrollable input due to the incoming wave field (i.e. the wave excitation force), we incorporate a combined state and input observer based on an augmented Kalman-Bucy filter. The combination of LTI energy-maximising controller, state/input observer, and proposed AW technique, is tested experimentally, using a prototype of the Wavestar system, within the experimental facilities available at Aalborg University. We effectively demonstrate that the proposed AW scheme is able to consistently respect the defined state constraints in practice, having a mild impact on the overall energy absorption performance. Further studies with this technique will focus in a experimental comparison of this technique with optimisation-based strategies, such as e.g., MPC, including any corresponding formal analysis with respect to the associated closed-loop properties.

References

[1] N. Faedo, D. García-Violini, Y. Peña-Sanchez, and J. V. Ringwood, "Optimisation-vs. non-optimisation-based energy-maximising control for wave energy converters: A case study," in *Proc. IEEE Eur. Control Conf.*, 2020, pp. 843–848.

[2] N. Faedo, S. Olaya, and J. V. Ringwood, "Optimal control, MPC and MPC-like algorithms for wave energy systems: An overview," *IFAC J. Syst. Control*, vol. 1, pp. 37–56, 2017.

[3] G. Li and M. R. Belmont, "Model predictive control of sea wave energy converters–part I: A convex approach for the case of a single device," *Renewable Energy*, vol. 69, pp. 453–463, 2014.

[4] Y. Jia, K. Meng, L. Dong, T. Liu, C. Sun, and Z. Y. Dong, "Economic model predictive control of a point absorber wave energy converter," *IEEE Trans. Sustain. Energy*, vol. 12, no. 1, pp. 578–586, Jan. 2021.

[5] G. Bacelli and J. V. Ringwood, "Numerical optimal control of wave energy converters," *IEEE Trans. Sustain. Energy*, vol. 6, no. 2, pp. 294–302, Apr. 2015.

[6] R. Genest and J. V. Ringwood, "Receding horizon pseudospectral control for energy maximization with application to wave energy devices," *IEEE Trans. Control Syst. Technol.*, vol. 25, no. 1, pp. 29–38, Jan. 2017.

[7] N. Faedo, F. Carapellese, E. Pasta, and G. Mattiazzo, "On the principle of impedance-matching for underactuated wave energy harvesting systems," *Appl. Ocean Res.*, vol. 118, 2022, Art. no. 102958.

[8] D. García-Violini, N. Faedo, F. Jaramillo-Lopez, and J. V. Ringwood, "Simple controllers for wave energy devices compared," *J. Mar. Sci. Eng.*, vol. 8, no. 10, 2020, Art. no. 793.

[9] F. Fusco and J. V. Ringwood, "A simple and effective real-time controller for wave energy converters," *IEEE Trans. Sustain. Energy*, vol. 4, no. 1, pp. 21–30, Jan. 2013.

[10] D. García-Violini, Y. Peña-Sanchez, N. Faedo, C. Windt, F. Ferri, and J. V. Ringwood, "Experimental implementation and validation of a broad-band LTI energy-maximizing control strategy for the wavestar device," *IEEE Trans. Control Syst. Technol.*, vol. 29, no. 6, pp. 2609–2621, Nov. 2021.

[11] A. H. Glattfelder and W. Schaufelberger, *Control Systems With Input and Output Constraints*, vol. 1. Berlin, Germany: Springer, 2003.

[12] A. H. Glattfelder and W. Schaufelberger, "A path from antiwindup to override control," *IFAC Proc. Volumes*, vol. 37, no. 13, pp. 1099–1104, 2004.

[13] E. Chambon, L. Burlion, and P. Apkarian, "Time-response shaping using output to input saturation transformation," *Int. J. Control*, vol. 91, no. 3, pp. 534–553, 2018.

[14] O. J. Rojas and G. C. Goodwin, "A simple anti-windup strategy for state constrained linear control," *IFAC Proc. Volumes*, vol. 35, no. 1, pp. 109–114, 2002.
[15] R. H. Hansen and M. M. Kramer, "Modelling and control of the wavestar prototype," in *Proc. 9th Eur. Wave Tidal Energy Conf.*, 2011, pp. 1–10.
[16] N. Faedo, Y. Peña-Sanchez, E. Pasta, G. Papini, F. D. Mosquera, and F. Ferri, "SWELL: An open-access experimental dataset for arrays of wave energy conversion systems," *Renewable Energy*, vol. 212, pp. 699–716, 2023.
[17] J. Ringwood et al., "A competition for WEC control systems," in *Proc. 12th Eur. Wave Tidal Energy Conf.*, 2017, pp. 1–9.
[18] J. Ringwood et al., "The wave energy converter control competition: Overview," in *Proc. Int. Conf. Offshore Mechanics Arctic Eng.*, 2019, Art. no. V010T09A035.
[19] J. Scruggs, "On the causal power generation limit for a vibratory energy harvester in broadband stochastic response," *J. Intell. Mater. Syst. Struct.*, vol. 21, no. 13, pp. 1249–1262, 2010.
[20] N. Faedo et al., "Energy-maximising experimental control synthesis via impedance-matching for a multi degree-of-freedom wave energy converter," *IFAC-PapersOnLine*, vol. 55, no. 31, pp. 345–350, 2022.
[21] G. Bacelli and J. V. Ringwood, "A geometric tool for the analysis of position and force constraints in wave energy converters," *Ocean Eng.*, vol. 65, pp. 10–18, 2013.
[22] S. Galeani, S. Tarbouriech, M. Turner, and L. Zaccarian, "A tutorial on modern anti-windup design," in *Proc. Eur. Control Conf.*, 2009, pp. 306–323.
[23] Y. Peña-Sanchez, C. Windt, J. Davidson, and J. V. Ringwood, "A critical comparison of excitation force estimators for wave-energy devices," *IEEE Trans. Control Syst. Technol.*, vol. 28, no. 6, pp. 2263–2275, Nov. 2020.
[24] R. E. Kalman and R. S. Bucy, "New results in linear filtering and prediction theory," *J. Basic Eng.*, vol. 83, no. 1, pp. 95–108, 1961.
[25] A. Mérigaud and J. V. Ringwood, "Free-surface time-series generation for wave energy applications," *IEEE J. Ocean. Eng.*, vol. 43, no. 1, pp. 19–35, Jan. 2018.
[26] N. Faedo, Y. Peña-Sanchez, D. Garcia-Violini, F. Ferri, G. Mattiazzo, and J. V. Ringwood, "Experimental assessment and validation of energy-maximising moment-based optimal control for a prototype wave energy converter," *Control Eng. Pract.*, vol. 133, 2023, Art. no. 105454.
[27] L. Ljung, "System identification," in *Signal Analysis and Prediction*. Berlin, Germany: Springer, 1998, pp. 163–173.
[28] P. Van Overschee and B. De Moor, "Continuous-time frequency domain subspace system identification," *Signal Process.*, vol. 52, no. 2, pp. 179–194, 1996.
[29] N. Faedo, Y. Peña-Sanchez, F. Carapellese, G. Mattiazzo, and J. V. Ringwood, "LMI-based passivation of LTI systems with application to marine structures," *IET Renewable Power Gener.*, vol. 15, no. 14, pp. 3424–3433, 2021.

Nicolás Faedo was born in Buenos Aires, Argentina, in 1991. He received the Degree in automation and control engineering from the National University of Quilmes, Buenos Aires, Argentina, in 2015, and the Ph.D. degree in electronic engineering from the Centre for Ocean Energy Research group, Maynooth University, Kildare, Ireland, in 2020, with a focus on optimal control and model reduction for wave energy converters from a system-theoretic perspective. In 2017, he joined the Centre for Ocean Energy Research group, Maynooth University. In 2018, he was a Visiting Researcher multiple times with the Control and Power Group, Imperial College London, London, U.K. He currently holds a Postdoctoral position with the Department of Mechanical and Aerospace Engineering, Politecnico di Torino, Turin, Italy. His research interests include nonlinear optimal control theory and data-driven model reduction, with special emphasis in applications involving renewable energy systems. Dr. Faedo was the recipient of the Marie Skłodowska-Curie Actions Individual Fellowship (MSCA-IF 2020), 2022 IFAC CAMS Best Paper Award, 2019 ISOPE Best Student Paper Award and the Exxonmobile Prize, and finalist for the 2018 IFAC CAMS Young Author Award. He has been selected an Outstanding Reviewer two years in a row (2020-2021) for the IEEE TRANSACTIONS ON SUSTAINABLE ENERGY.

Fabio Carapellese was born in Andria, Italy in 1995. He received the B.Sc. degree in mechanical engineering in 2017 and the M.Sc. degree in mechatronic engineering in 2019 from Politecnico di Torino, Turin, Italy, where he is currently working toward the Ph.D. degree, with the Marine Offshore Renewable Energy Lab, focuses on dynamic design of inertial wave energy converter system. In 2020, he was a Visiting Researcher with the Wallace Energy Systems and Renewables Facility, Oregon State University, Corvallis, OR, USA. His research interests include multi-DoF modelling and control design of wave energy systems, with a particular focus on nonlinear behavior. In 2022, he was the recipient of the 2022 IFAC CAMS Best Paper Award.

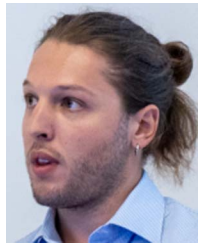

Guglielmo Papini (Graduate Student Member, IEEE) was born in Florence, Italy in 1997. He received the B.Sc. degree in mechanical engineering from Università degli Studi di Firenze, Florence, Italy, and the M.Sc. degree in mechatronic engineering in 2019 and 2021, respectively, from Politecnico di Torino, Turin, Italy, where he is currently working toward the Ph.D. degree with Marine Offshore Renewable Energy Lab, focuses on fault detection and fault-tolerant control of wave energy converters.

Edoardo Pasta (Graduate Student Member, IEEE) was born in Turin, Italy in 1996. He received the B.Sc. degree in mechanical engineering in 2018 and the M.Sc. degree in mechatronic engineering in 2020 from Politecnico di Torino, Turin, Italy, where he is currently working toward the Ph.D. degree with Marine Offshore Renewable Energy Lab, focuses on optimal control and modeling of wave energy converters. In 2020, he was a Visiting Researcher with the Computational Fluid Dynamics and Flow Physics Laboratory, San Diego State University, San Diego, CA, USA. Between 2021 and 2022, he joined the Centre for Ocean Energy Research, Maynooth University, Kildare, Ireland, as a Visiting Researcher. His research interests include optimal control and modeling of wave energy systems, with a particular focus on data-based and data-driven techniques. In 2022, he was the recipient of the 2022 IFAC CAMS Best Paper Award.

Facundo D. Mosquera received the Bachelor of Science degree in electronic engineering and the Ph.D. degree from the Universidad Nacional de La Plata (UNLP), La Plata, Argentina, in 2017 and 2023, respectively. He is currently a Teaching Assistant with the Department of Electrical Engineering, UNLP. His research focuses on automatic control, with a specific emphasis on its applications in renewable energy systems, notably wave energy converters.

Francesco Ferri received the master's degree in chemical and process engineering from the University of Bologna, Bologna, Italy, in 2008, and the Ph.D. degree in experimental and numerical modelling of wave energy converters from Aalborg University, Aalborg, Denmark. He is currently an Associate Professor of offshore engineering with Aalborg University. His research interests include experimental and numerical modeling, hydrodynamic interaction in renewable energy offshore parks, and control of wave energy converters.

Ted K. A. Brekken (Senior Member, IEEE) received the B.S., M.S., and Ph.D. degrees from the University of Minnesota, Minneapolis, MN, USA, in 1999, 2002, and 2005 respectively. He is currently a Professor of energy systems with Oregon State University, Corvallis, OR, USA. Duirng 2004–2005, he studied wind turbine control with the Norwegian University of Science and Technology, Trondheim, Norway, on a Fulbright scholarship. His research interests include control and modeling of renewable energy systems and electrical system resilience. He is the Co-Director of the Wallace Energy Systems and Renewables Facility. He was the recipient of the NSF CAREER Award, IEEE Power and Energy Outstanding Young Engineer Award, and numerous teaching awards.